Assessing the wall effects of backwards-facing step flow in tightly-coupled experiments and simulations

Julian Toumey *, Peiyu Zhang †, and Xinyu Zhao ‡
University of Connecticut, Storrs, CT, 06269, USA

Jennifer Colborn§ and Jacqueline O'Connor¶
Pennsylvania State University, University Park, PA, 16802, USA

Backward facing steps are found in a range of engineering applications, including combustors, which is the main focus of the current work. Backwards facing steps promote shear generation and recirculation, as the boundary layer that develops ahead of the step separates and flow reverses behind the step. At the end of the recirculation zone, the shear layer impinges on the bottom wall of the step and the flow recovers, forming a new boundary layer downstream. When a flame is present in this configuration, it stabilizes in the shear layer, impinging on the wall downstream of the step. This flame configuration results in complex convective and radiative heat transfer to the wall. In this study, we begin investigations of these different heat transfer mechanism to the wall downstream of the backwards facing step using both experiments and large eddy simulations. In order to promote accurate comparisons between the experiments and simulation, we have first considered the spanwise variation of the velocity fields in the experiment. The experiment was designed such that the wall effects should be minimal along the centerline of the experiment, and large eddy simulations of the non-reacting flow show this is the case. Direct comparisons between these simulation results and preliminary velocity measurements from a particle image velocimetry technique show reasonably good agreement.

I. Nomenclature

γ	=	mesh grading function parameter
h	=	step height
h_c	=	inlet channel height
ν_t	=	turbulent (eddy) viscosity
x, y, z	=	streamwise, wall-normal, and spanwise directions coordinate, respectively
X_R	=	recirculation zone length

II. Introduction

Backward facing steps are ubiquitous in a range of engineering applications, including combustors, which is the main focus of this study and several others [1, 2]. The shear layer that forms due to the presence of the step impinges on the bottom wall, forming a recirculation region upstream and a new boundary layer downstream. The recirculation zone and shear layer serve to stabilize the flame and also drive complex convective and radiative heat transfer to the wall. The backward-facing step combustor captures critical combustor flow field features–high turbulence intensity, recirculation, shear layer separation, and shear layer impingement–in a two-dimensional configuration that is optimal for diagnostic access from all sides.

A significant gap in the literature is the insufficient amount of studies that consider combustor liner heat transfer

*Graduate Research Assistant, Mechanical Engineering, AIAA Student Member
†Graduate Research Assistant, Mechanical Engineering, AIAA Student Member
‡Associate Professor, Mechanical Engineering, AIAA Member
§Graduate Research Assistant, Mechanical Engineering, AIAA Student Member
¶Associate Professor, Mechanical Engineering, AIAA Associate Fellow

accounting for both convection and radiation, particularly with a flame present. Most studies of combustor liner heat transfer are non-reacting studies, focusing on convective heat transfer and the performance of liner cooling strategies. In particular, a large literature on effusion cooling and the impact of the combustor flow field on the effusion layer highlights the importance of the combustor flow field on liner heat transfer [3–6]. While the current work does not include effusion cooling, some of the learning from this literature is pertinent. Tarchi et al. [5] investigated the impact of recirculation on liner heat transfer with effusion cooling. They found that wall heat transfer was reduced by recirculation but augmented by the impingement of the shear layer on the wall downstream of the recirculation zone. This finding mirrors studies of heat transfer in backward-facing steps [7], where heat transfer and friction coefficient are enhanced downstream of the recirculation zone. Work by Ge et al. [8] showed that the heat transfer at the shear layer impingement location is greater with a flame. This enhancement is likely because the flame is stabilized in the shear layer and is a source of high temperature gases, although this study did not provide detail about the mechanisms by which flow features and the flame influenced liner heat transfer. Recent work by Park et al. [9] that measured wall temperatures in a swirl-stabilized combustor configuration also illustrated the importance of flame impingement on the wall, showing a significant increase in combustor liner heat flux downstream of the flame impingement location as convective heating by hot gases drove heat transfer to the wall.

Large eddy simulation (LES) from CERFACS has investigated liner heat transfer in a simulation that accounts for both convection and radiation [6]. These studies investigated the sensitivity of the liner heat flux to inclusion of different heat transfer effects, namely convection vs. radiation, in a helicopter engine with backside cooling but no effusion cooling. The authors identified regions of recirculation as being locations of augmented heat transfer, and showed that in this geometry, the integrated heat fluxes from radiation and convection were of similar magnitude, indicating that accurate prediction of wall temperatures requires consideration of radiation at engine conditions. Many of these initial studies, both experimental and numerical, included a large number of realistic effects: effusion cooling, swirling flows, realistic liner geometries, etc. As a result, however, it is difficult to extract fundamental relationships between different key operational parameters that drive heat flux to the wall.

The issue of combustor liner heat transfer mechanisms will be addressed through studying the backward facing step combustor described in this work. The experimental design is motivated by the need to capture important combustor flow features while maintaining access for high-fidelity, simultaneous measurements. Both these goals can be achieved through the use of a backwards-facing step combustor, which has been used extensively in combustion research [1, 2, 10]. The backwards-facing step combustor captures critical combustor flow field features – turbulent flow, recirculation, shear layer separation, and shear layer impingement – in a two-dimensional configuration. A two-dimensional geometry allows for better diagnostic access, where simultaneous measurements are critical to achieving the goals of the proposed work. Further, simulation of this configuration and comparison to experimental data will be more straightforward in a two-dimensional geometry. The goal of this paper is to compare the flow fields from the new experiment and the simulation using a reduced simulation domain. As will be explained in the next section, the combustor design features a wide combustor to ensure two-dimensionality along the centerline for comparison to simulation. However, this combustor geometry is too large for tractable high-fidelity simulation, and so a reduced domain is proposed. We compare the results from the reduced domain with those of the experiment, showing good agreement between the experimental and simulation results, supporting the use of the reduced domain for future heat transfer studies.

III. Experimental Description

Figure 1 shows the current experiment setup. The combustor facility consists of three sections: the pre-conditioning section, the combustor, and the exhaust. At reacting conditions, a mixture of fuel and air first burns in a small vitiator, achieving high temperatures without combustion in the main combustor and allowing for important comparisons between operating conditions with and without a flame. To modulate the temperature in the main test section, additional cold air can be added downstream of the vitiator. Turbulence generating plates increase the turbulence intensity of the flow entering the test section. The test section consists of a backward-facing step combustor with optical access on three sides. Downstream of the step is the main combustor section with an instrumented bottom wall and a window on the top. The top and side windows extend from upstream of the step to the end of the test section for measurement of the flow both upstream and downstream of the step. The bottom wall of the combustor is interchangeable, from a thin metal wall, appropriate for measuring back-side temperature profiles, to a thick wall with heat flux instrumentation.

Sizing of the backwards-facing step combustor is consistent with previous designs for combustion applications. As demonstrated by Broderode [11], an aspect ratio of 10 was needed to have two-dimensional flow along the centerline, where the aspect ratio is defined as the cross-stream step width divided by the step height. In a two-dimensional

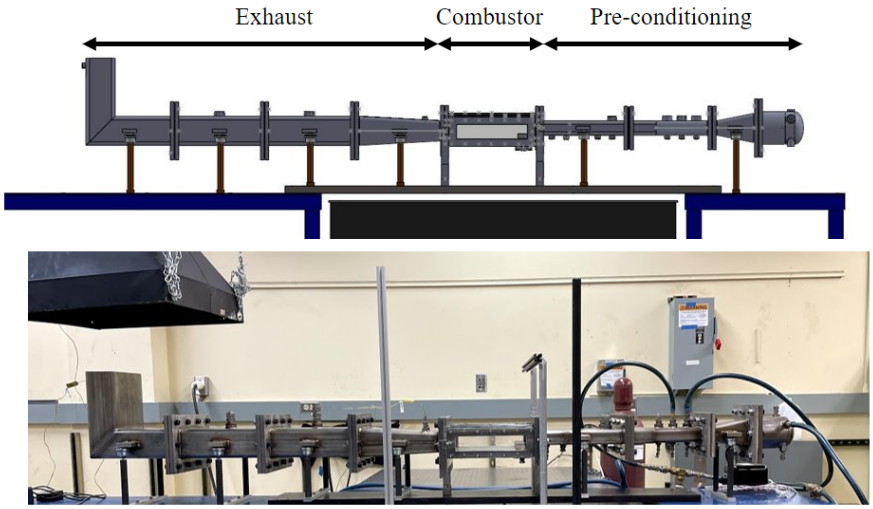

Fig. 1 A schematic of the experimental configuration.

configuration, time-averaged shear layer reattachment lengths of 6-8 step heights were shown by Eaton and Johnston [12], which dictated the length of the combustor. Additionally, Eaton and Johnston showed the expansion ratio, which is the channel height after the step divided by the channel height before the step, was normally between 1 and 1.6, but as large as 2 has been used by Ghoniem et al. [10].

Using these parameters, the step height was selected to be 2 cm, the aspect ratio 10, the expansion ratio to be 1.5, and the channel is 12 step heights long to ensure full reattachment was visible. This sizing resulted in initial combustor dimensions of 6 cm high by 30 cm long by 20 cm wide, with a step that was 6 cm long and 2 cm high. The combustor dimensions were adjusted to better fit prefabricated imperial unit tubing, and while the step size stayed the same the combustor became 5.8 cm high by 30 cm long by 19 cm wide. While the new aspect ratio with these dimensions is slightly below the 10 that Broderode detailed, others have used values slightly lower and still maintained the two-dimensionality assumption [13]. The efficacy of this aspect ratio at ensuring two-dimensionality along the centerline is tested in this work.

IV. Methods

A. Computational methods

For the computational portion of the study, only the combustion chamber is simulated as illustrated in Fig. 2. Large-eddy simulations (LES) are performed for the non-reacting configuration using the open-source CFD package `OpenFOAM` [14] with in-house sub-models. The solver is an incompressible solver which employs a modified PISO algorithm for pressure-velocity coupling. Spatial discretization is second-order and time advancement is handled via the first-order Euler integration scheme. The Dynamic Smagorinsky sub-grid model is implemented [15] to model the subgrid-scale stress.

To represent the turbulent fluctuations present at the inlet, velocity and turbulence statistics profiles extracted from the DNS of Spalart are supplied [16] in conjunction with the method of random spots to impose velocity fluctuations with a prescribed energy spectrum [17]. Measurements from the experimental group will replace this method when available.

The boundary conditions used for the simulation are illustrated in Fig. 2 and described in Table 1. As discussed below, the simulation is wall-resolved and hence no-slip boundary conditions are used for velocity at the wall. Turbulent viscosity is reduced to be zero at the wall. For the reduced span simulations, spanwise boundary conditions were replaced with periodic conditions, indicating that the selected span was independent of effects from the span walls.

Preliminary work indicates that wall-resolved LES (WRLES) is feasible for the case. Therefore, the mesh is designed

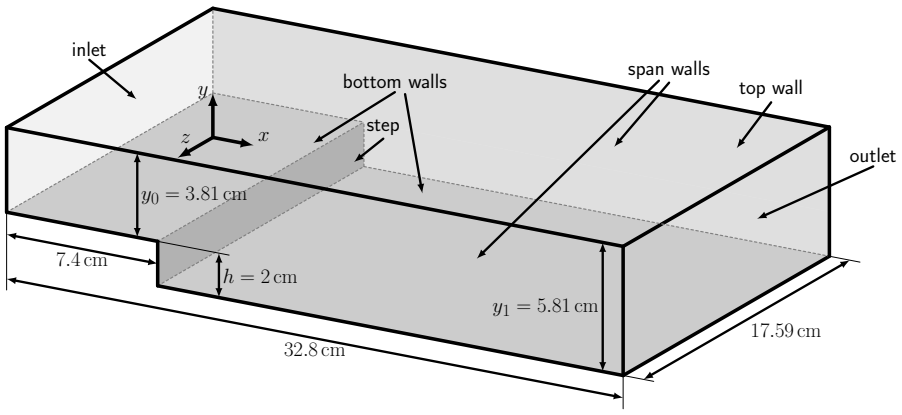

Fig. 2 Illustration of the computational domain used for non-reacting combustor simulations with dimensions and corresponding boundary conditions.

Table 1 Boundary conditions employed in the non-reacting simulations. Descriptions in parenthesis indicate boundary conditions used for reduced span simulations.

Boundary	Velocity	Pressure	Turbulent Viscosity
inlet	Inflow generator ([17])	Neumann	Neumann
outlet	Neumann	Total pressure	Neumann
span walls	No-slip (periodic)	Neumann (periodic)	Dirichlet (periodic)
top wall	No-slip	Neumann	Dirichlet
step	No-slip	Neumann	Dirichlet
bottom walls	No-slip	Neumann	Dirichlet

to achieve sufficient near-wall resolution such that the $y+$ is on the order of one, obviating the need for algebraic wall models. Cell sizes in the wall-normal direction are determined using the hyperbolic tangent function of Gullbrand:

$$y(j) = -\frac{\tanh\left(\gamma(1 - 2j/N_2)\right)}{\tanh\left(\gamma\right)} \tag{1}$$

in which y represents the wall-normal cell center location, j the cell index, N_2 the number of cells in the wall-normal direction, and γ a grading parameter which was set to 2.75 [18].

Figure 3 displays the near-wall velocity in dimensionless wall coordinates after 20 flow-throughs at successive locations along the inlet channel. In addition to the number of cells clustered in the viscous sub-layer, one may observe the profiles collapsing to the log-law as the flow develops along the inlet channel. *A posteriori* analysis of the simulation indicated that the $y+$ for all channel walls was on the order of one or less.

Flow is simulated for 20 flow-through times based on the bulk convective velocity with statistics collected beginning at 10 flow-through times so as to allow initial transients to flush out of the domain.

B. Experimental methods

For initial combustor characterization, only cold flow was used. Air is metered with a thermal mass flow meter and then split into two streams. Most of the air was injected through the vitiator, with approximately 16% of the air flow by volume through the seeder. Alumina oxide particles with average diameter of 0.5-2 microns were injected about eight inches upstream of the test section. A flow condition of Re_h = 8000 was selected, where the Reynolds number is calculated using the step height as shown in Equation 2.

$$\text{Re}_\text{h} = \frac{\rho v h}{\mu} \tag{2}$$

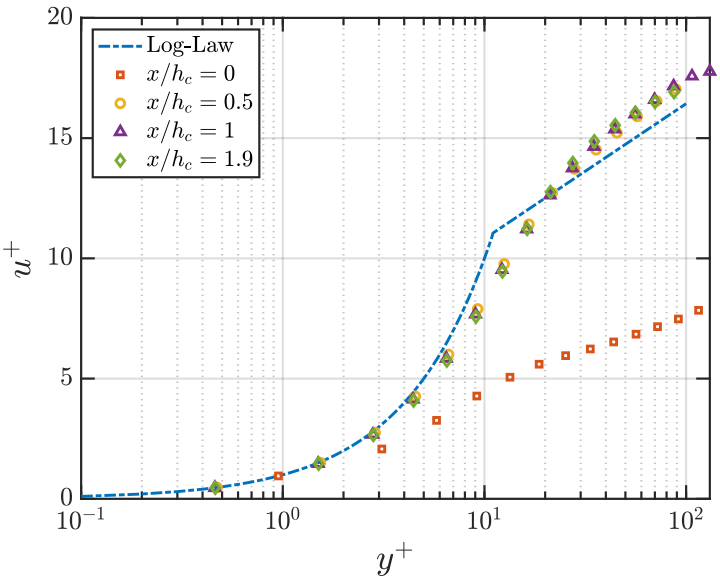

Fig. 3 ***A posteriori*** **illustration of near-wall velocity along the inlet channel in dimensionless wall coordinates for the fully-turbulent case. The step is located at x/h_c = 1.94. Velocity profiles are shown after 20 convective flow-through times.**

Velocity data is obtained using a high-speed particle image velocimetry system. Due to the limited width of the laser sheet, the laser sheet was moved multiple times within the combustor to fully capture the flow field at each location. Five fields of view along the length of the combustor were obtained and a composite image was created for each of the imaging planes. The PIV system consists of a Nd:YAG laser (Quantronix Hawk Duo) operating at 532 nm. The laser sheet at each condition is created using a combination of mirrors and a LaVision sheet forming optic; the angle between the laser sheet plane and each camera sensor (Photron FASTCAM SA1.1) is 90 degrees. The camera is equipped with a 60 mm f/2.8 lens (AF Micro Nikon). Images are collected at 5 kHz in double frame mode with a pulse separation of 80 μs. Aluminum oxide particles of diameters 0.5-2.0 μm are used for seeding the flow field. A laser line filter (Edmund Optics TECHSPEC 532 nm CWL) was used to eliminate ambient light from the images.

LaVision's DaVis 8.3 is used to perform vector calculations from Mie scattering images. These calculations include a multi-pass algorithm with varying window sizes ranging from 64 x 64 to 16 x 16 and a 50% overlap. This results in a vector spacing of 0.48 mm/vector. A universal outlier detection scheme, with a 3x median filter, is used for post-processing of the vector fields. A total of 5000 vector fields are obtained for each condition.

To match the computational work presented here, velocity profiles were gathered at three locations: the midplane, as well as two cross-stream locations (4 cm) on either side of the centerline, as shown in Figure 4. The off-center locations align with the reduced span used in simulations. The resolution of the imaging changed slightly between each of the planes, with a vector spacing of 1.02 mm for Plane 1, 1.13 mm for Plane 2, and 1.25 mm for Plane 3.

V. Results and Discussion

A. Numerical results

LES are performed at the Reynolds number based on step height of $\mathrm{Re_h} = 8,000$ (the maximum $\mathrm{Re_h}$ to be used in this study) on full and reduced span geometries. The full spanwise case includes no-slip wall boundary conditions in the span direction. The reduced span geometry employs periodic boundary conditions in the spanwise direction with a span width of four times the step height. Studies of Arnal and Freidrich indicate that the effect of spanwise periodic boundary conditions is diminished at this width [19]. Further, this span width is commonly employed for LES and DNS [20, 21].

Recirculation zone measurements are compared between the full and reduced span cases to assess the two-dimensional nature of the problem and the effect of the spanwise walls on certain computed statistics. Table 2 summarizes the

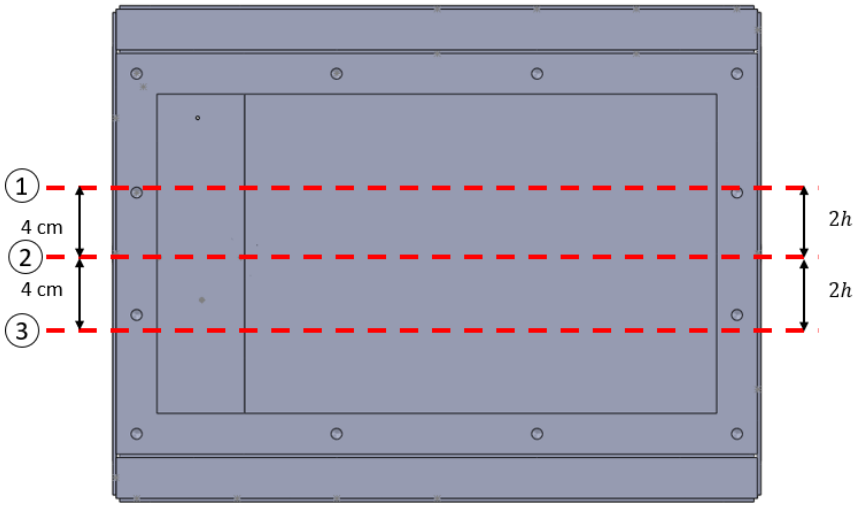

Fig. 4 PIV imaging planes as viewed from above the combustor, with flow from left to right. Plane 1 is closest to the camera.

recirculation zone measurements as compared between full and reduced span simulations. The mid-span measurements determine the recirculation zone extent by the maximum streamwise extent of zero time-averaged streamwise velocity. For span-averaged measurements, spanwise averaging of the time-averaged streamwise velocity is performed and the recirculation zone extent is determined by the zero streamwise velocity contour of this averaged value.

Clearly, truncating the span has little effect on the recirculation zone extent for this simulation configuration. Further, the measurement at the mid-span is in excellent agreement with the span-averaged value, indicating that at this maximum Reynolds number for this configuration (and the Reynolds numbers below this value), it is appropriate for the experimentalists to use the mid-span as the measurement location (TPIV, pressure taps, and thermocouples).

Additionally, it is appropriate for the computational group to use periodic boundary conditions and a truncated span because doing so does not significantly affect the metrics of interest and reduces the computational cost by a factor of approximately two. Figure 5 provides an illustration of these two measurement methods via the solid contour lines.

Table 2 Comparison of the length of the recirculation zones obtained from the full-span and reduced-span simulations.

Case	X_R Midspan	X_R Averaged Midspan
Full span	$6.44h$	$6.46h$
Reduced span	$6.52h$ (+1.2%)	$6.62h$ (+2.5%)

B. Experimental results and comparison with simulation

Time-averaged PIV results were collected and are shown below in Figures 6 through 8. Five thousand image pairs were taken and time-averaged at each location. In the figures, pink lines indicate edges of each field of view, and the white line is the zero axial velocity contour, which represents the border of the recirculation zone. Any areas greyed out had high reflections or poor lighting, resulting in data loss.

As can be seen in Figures 6 and 7, a distinct recirculation zone can be seen in the velocity profiles, as well as a relatively high velocity region over the top of the step and that slightly dissipates downstream. Additionally, similar velocity profiles and recirculation zone length is seen despite the difference in location in the flow. As shown in Table 3, Planes 1 and 2 show recirculation zone around 5 step heights downstream of the step end.

The recirculation zone for Plane 3 did not show as good agreement. Rather, a much shorter length is seen, closer to

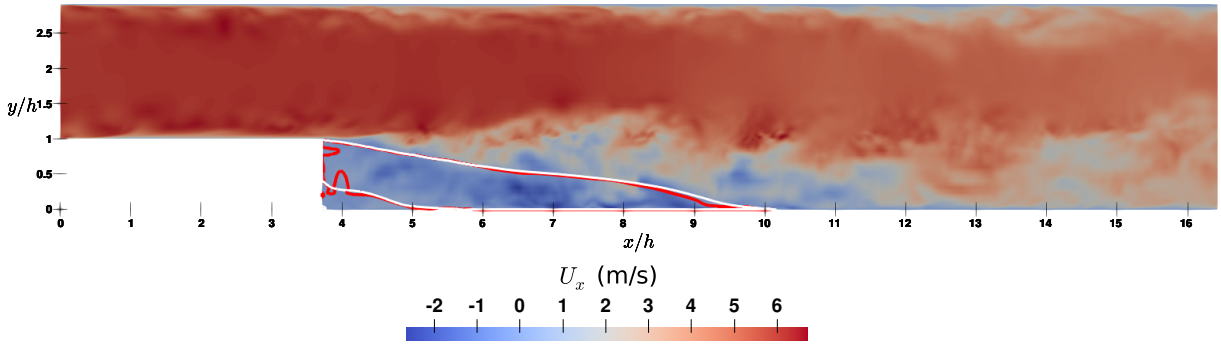

(a) Instantaneous streamwise velocity.

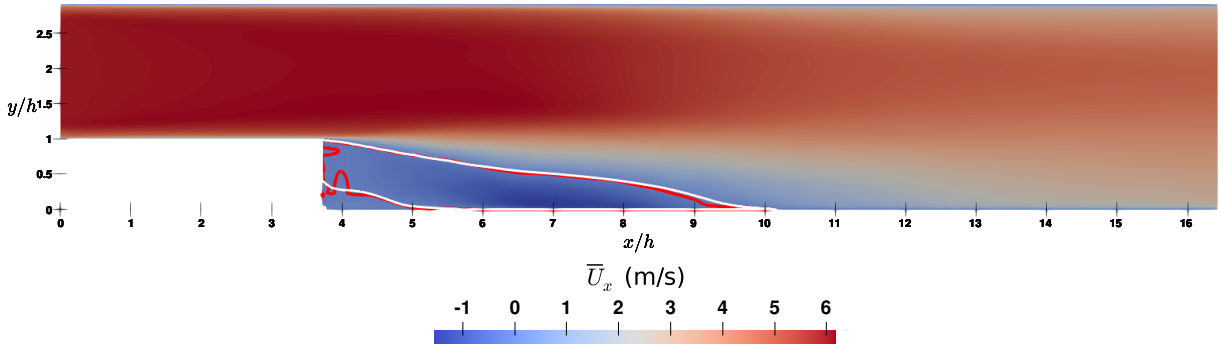

(b) Mean streamwise velocity.

Fig. 5 Instantaneous and time-averaged streamwise velocity. Red contour: X_R from mid-plane time-averaged velocity field, white contour (thicker): X_R from span-averaged time-averaged velocity field.

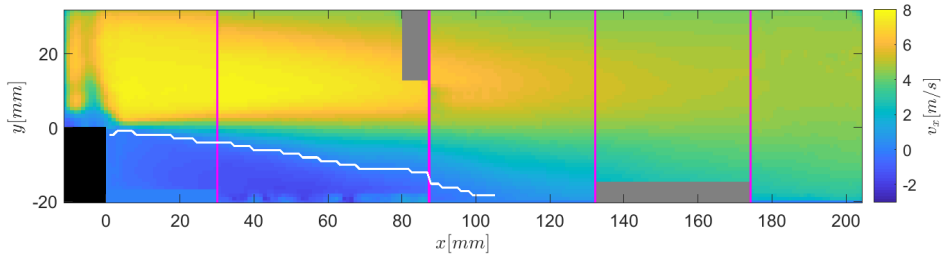

Fig. 6 Plane 1 velocity field. Pink lines indicate field of view boundaries for PIV, and grey boxes represent regions where data was not available. White contour is the zero axial-velocity contour, representing the boundary of the recirculation zone.

4 step heights. Further investigation is required at this time to determine if flow irregularities exist or if misalignment during PIV collection could have occurred, biasing results. The second and third data collection regions from the left in 8 have relatively lower velocities than those around it indicating a collection error could have occurred.

Comparison between the experimental and computational results shows similar profiles, but with discrepancy in magnitude. Agreement between experimental locations one and two indicates two dimensional flow through part of the combustor, which supports the truncated span used by the computational group.

Figure 9 compares time-averaged streamwise velocity profiles at four stations downstream of the step. In general,

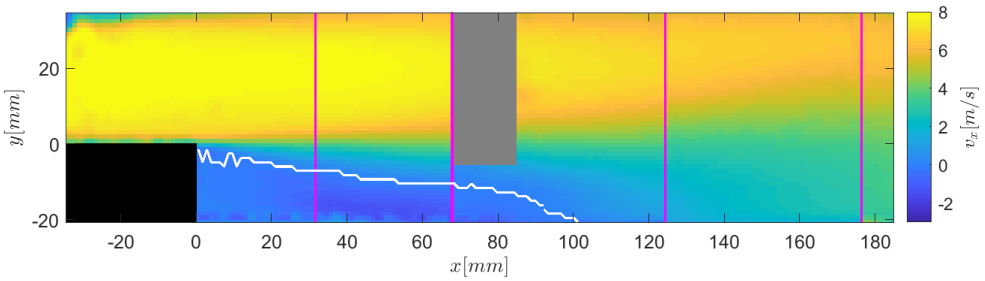

Fig. 7 Plane 2 velocity field.

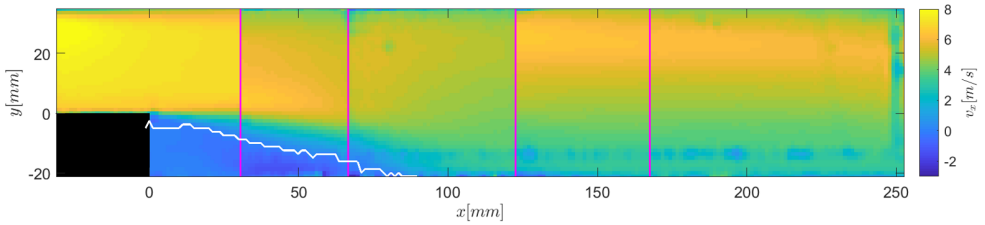

Fig. 8 Plane 3 velocity field.

there is qualitative agreement in the shapes of the profiles recorded in the LES and experiment. Experimental results indicate a slightly higher magnitude in the portion above the shear layer which may be attributable to the approximations used for turbulence intensity at the inlet for the LES. Additionally, the inlet turbulence statistics did not include a turbulent shear stress term which is quite significant in this type of free-shear flow. Further LES will use turbulence statistics recorded in the experimental investigation.

VI. Conclusions

Tightly-coupled experiments and large eddy simulations are conducted to study convection and radiative heat transfer in a backward-facing step combustor. The comparison between the reduced-span simulation and the full-span simulation indicate that two-dimensionality is a sufficient assumption for the target backward-facing step combustor. Reasonably good agreement between the experiments and simulation indicate that the reduced-span simulations are sufficient for capturing the behavior of the flow field at the target operating conditions. Future work will include the use of thermographic particle image velocimetry to determine simultaneous velocity and temperature statistics for comparison to simulation, and determination of the convective and radiative heat transfer to the liner wall at a variety of gas temperatures and flow rates.

Acknowledgments

The authors acknowledge financial support through the Office of Naval Research, Grant N00014-20-1-2278, with program monitor Dr. Steven Martens. The computational resources are provided in part by the DoD High Performance Computing Modernization Program.

References

[1] Altay, H. M., Speth, R. L., Hudgins, D. E., and Ghoniem, A. F., "Flame–vortex interaction driven combustion dynamics in a backward-facing step combustor," *Combustion and Flame*, Vol. 156, No. 5, 2009, pp. 1111–1125.

[2] McManus, K., Vandsburger, U., and Bowman, C., "Combustor performance enhancement through direct shear layer excitation," *Combustion and Flame*, Vol. 82, No. 1, 1990, pp. 75–92.

[3] Scrittore, J. J., Thole, K. A., and Burd, S. W., "Investigation of Velocity Profiles for Effusion Cooling of a Combustor

Table 3 Experimental recirculation zone locations.

Case	$X_R[mm]$	$X_R/h[-]$
1	105.2	5.26
2	101.2	5.06
3	84.65	4.23

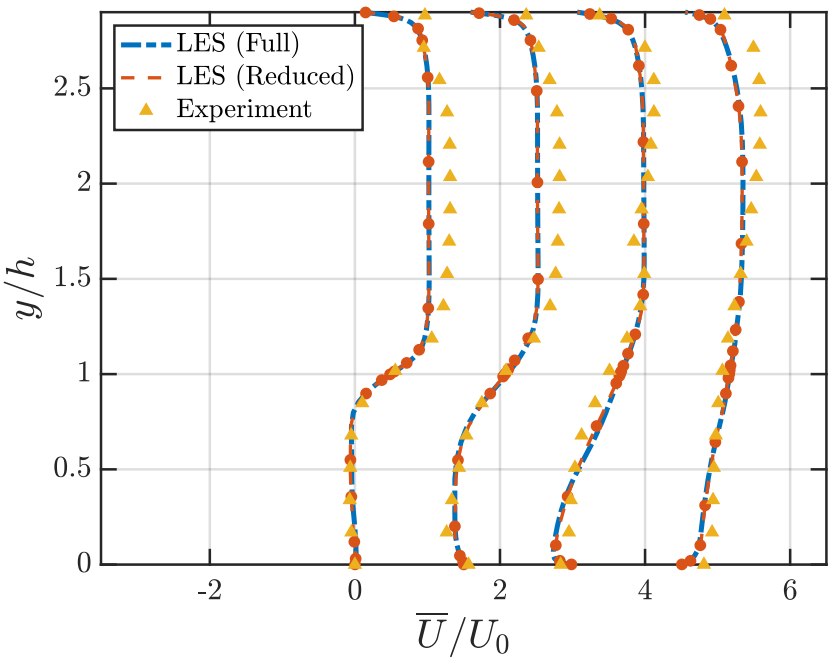

Fig. 9 Comparison of time-averaged streamwise velocity $\overline{U}_x$ normalized by bulk velocity U_0 between LES (full- and reduced-span) and experiment. From left to right, curves are located at $x/h = 1,\ 2,\ 4\ 8$ downstream of the step. Each curve is successively offset by $1.5\,\overline{U}_x/U_0$ for visibility.

Liner," *Journal of Turbomachinery*, Vol. 129, No. 3, 2006, pp. 518–526. https://doi.org/10.1115/1.2720492, URL https://doi.org/10.1115/1.2720492.

[4] Andreini, A., Becchi, R., Facchini, B., Mazzei, L., Picchi, A., and Turrini, F., "Adiabatic effectiveness and flow field measurements in a realistic effusion cooled lean burn combustor," *Journal of Engineering for Gas Turbines and Power*, Vol. 138, No. 3, 2016.

[5] Tarchi, L., Facchini, B., Maiuolo, F., and Coutandin, D., "Experimental investigation on the effects of a large recirculating area on the performance of an effusion cooled combustor liner," *Journal of engineering for gas turbines and power*, Vol. 134, No. 4, 2012.

[6] Berger, S., Richard, S., Staffelbach, G., Duchaine, F., and Gicquel, L., "Aerothermal prediction of an aeronautical combustion chamber based on the coupling of large eddy simulation, solid conduction and radiation solvers," *ASME Turbo Expo 2015: Turbine Technical Conference and Exposition*, American Society of Mechanical Engineers Digital Collection, 2015.

[7] Vogel, J. C., and Eaton, J. K., "Combined Heat Transfer and Fluid Dynamic Measurements Downstream of a Backward-Facing Step," *Journal of Heat Transfer*, Vol. 107, No. 4, 1985, pp. 922–929. https://doi.org/10.1115/1.3247522, URL https://doi.org/10.1115/1.3247522.

[8] Ge, B., Ji, Y., Chi, Z., and Zang, S., "Effusion cooling characteristics of a model combustor liner at non-reacting/reacting flow conditions," *Applied Thermal Engineering*, Vol. 113, 2017, pp. 902–911.

[9] Park, S., Gomez-Ramirez, D., Gadiraju, S., Kedukodi, S., Ekkad, S. V., Moon, H.-K., Kim, Y., and Srinivasan, R., "Flow field and wall temperature measurements for reacting flow in a lean premixed swirl stabilized can combustor," *Journal of Engineering for Gas Turbines and Power*, Vol. 140, No. 9, 2018.

[10] Ghoniem, S., A.F.and Park, Wachsman, A., A., A., Wee, D., and Altay, H., "Mechanism of combustion dynamics in a backward-facing step stabilized premixed flame," *Proceedings of the Combustion Institute*, Vol. 30, 2005, pp. 1783–1790. https://doi.org/10.1016/j.proci.2004.08.201.

[11] Brederode, V., "Three-dimensional effects in nominally two-dimensional flows," Ph.D. thesis, Imperial College of Science and Technology, London University, 12 1974.

[12] Eaton, J., and Johnston, J., "A Review of Research on Subsonic Turbulent Flow Reattachment," *AIAA Journal*, Vol. 19, No. 9, 1981, pp. 1093–1100. https://doi.org/10.2514/3.60048.

[13] Kapiris, P., and Mathioulakis, D., "Experimental study of vortical structures in a periodically perturbed flow over a backward-facing step," *International Journal of Heat and Fluid Flow*, Vol. 47, 2014, pp. 101–112. https://doi.org/10.1016/j.ijheatfluidflow.2014.03.004.

[14] Weller, H. G., Tabor, G., Jasak, H., and Fureby, C., "A tensorial approach to computational continuum mechanics using object-oriented techniques," *Computers in Physics*, Vol. 12, No. 6, 1998, p. 620. https://doi.org/10.1063/1.168744.

[15] Germano, M., Piomelli, U., Moin, P., and Cabot, W. H., "A dynamic subgrid-scale eddy viscosity model," *Physics of Fluids*, Vol. 3, No. 7, 1991, pp. 1760–1765. https://doi.org/10.1063/1.857955.

[16] Spalart, P. R., "Direct simulation of a turbulent boundary layer up to R_θ= 1410," *Journal of Fluid Mechanics*, Vol. 187, 1988, pp. 61–98. https://doi.org/10.1017/S0022112088000345.

[17] Kornev, N., and Hassel, E., "Synthesis of homogeneous anisotropic divergence-free turbulent fields with prescribed second-order statistics by vortex dipoles," *Physics of Fluids*, Vol. 19, No. 6, 2007. https://doi.org/10.1063/1.2738607.

[18] Gullbrand, J., "Grid-independent large-eddy simulation in turbulent channel flow using three-dimensional explicit filtering," *Center for Turbulence Research Annual Research Briefs*, 2003.

[19] Arnal, M., and Freidrich, R., "On the effects of spatial resolution and subgrid-scale modeling in the large eddy simulation of a recirculating flow," *Notes on Numerical Fluid Mechanics: Proceedings of the Ninth GAMM-Conference on Numerical Methods in Fluid Mechanics.*, Vol. 35, 1991, pp. 3–13. https://doi.org/10.2307/2007976.

[20] Akselvoll, K., and Moin, P., "Large eddy simulation of turbulent confined coannular jet and turbulent flow over a backward-facing step," *Report TF-63, Thermosciences Division, Deptartment of Mechanical Engineering, Stanford University, California*, 1995.

[21] Le, H., Moin, P., and Kim, J., "Direct numerical simulation of turbulent flow over a backward-facing step," *Journal of Fluid Mechanics*, Vol. 330, 1997, pp. 349–374. https://doi.org/10.1017/S0022112096003941.